# This is the accepted manuscript version of the contribution published as:

Wang, Y., Shao, H., Kuhlman, K.L., Jove-Colon, C.F., **Kolditz, O.** (2024): Shear-induced fluid localization, episodic fluid release and porosity wave in deformable low-permeability rock salt *Geomech. Energy Environ.* **40**, art. 100600

### The publisher's version is available at:

https://doi.org/10.1016/j.gete.2024.100600

## Shear-induced fluid localization, episodic fluid release and porosity wave in deformable low-permeability rock salt

Yifeng Wang<sup>1\*</sup>, Hua Shao<sup>2</sup>, Kristopher L. Kuhlman<sup>1</sup>, Carlos F. Jove-Colon<sup>1</sup>, Olaf Kolditz<sup>3</sup>

**Abstract:** Understanding fluid distribution and migration in deformable low-permeability rock salt is critical for geologic disposal of nuclear waste. Field observations indicate that fluids in a salt formation are likely compartmentalized into relatively isolated patches and fluid release from such a formation is generally episodic. The underlying mechanism for these phenomena remains poorly understood. In this paper, a hydrological-mechanical model is formulated for fluid percolation in a rock salt formation under a deviatoric stress. Using a linear stability analysis, we show that a porosity wave (a train of alternating high and low porosity pockets) can emerge from positive feedbacks among intergranular wetting, grain boundary weakening and shear-induced material dilatancy. Fluid localization or episodic release can be viewed as a stationary or propagating porosity wave respectively. Fluid pockets transported via a porosity wave remain relatively isolated with minimal mixing between neighboring pockets. We further show that the velocity of fluid flow can be significantly enhanced by the emergence of a porosity wave. The concept and the related model presented in this paper provide a unified consistent explanation for the key features observed in fluid flow in rock salt. The similar process is expected to occur in other deformable low-permeability media such as shale and partially molten rocks under a deviatoric stress. Thus, the result presented here has an important implication to hydrocarbon expulsion from shale source rocks, radioactive waste isolation in a tight rock repository, and caprock integrity of a subsurface gas (CO<sub>2</sub>, H<sub>2</sub> or CH<sub>4</sub>) storage system. It may also help develop a new engineering approach to fluid injection into or extraction from unconventional reservoirs.

#### 1. Introduction

Bedded or domal salt formations have been considered as candidate host media for deep geologic disposal of nuclear waste due to their low permeability, low porosity, high thermal conductivity, and ability to close and heal crack openings<sup>1</sup>. Fluid migration in salt affects waste isolation in such media. Significant effort has been made to understand fluid flow in salt and the dependence of salt permeability on various environmental factors (temperature, pressure, and stress)<sup>2</sup>. The permeability of salt has been theorized using the concept of dihedral angle<sup>3</sup>. Lewis and Holness<sup>4</sup> experimentally determined the dihedral angle for an equilibrium halite-H<sub>2</sub>O system as a function of temperature and pressure and showed that, with a normal geothermal gradient in sedimentary basins, a halite body at a depth exceeding 3 km would have a low dihedral angle and thus could form a stable interconnected brine-filled porosity, leading to an increased permeability. Ghanbarzadeh et al.<sup>5</sup> analyzed wells penetrating salt deposits in the Gulf of Mexico and observed that fluid percolation would occur at larger dihedral angles (> 60°) for porosities considerably

<sup>&</sup>lt;sup>1</sup>Sandia National Laboratories, Albuquerque, New Mexico, USA

<sup>&</sup>lt;sup>2</sup>Federal Institute for Geosciences and Natural Resources, Hannover, Germany

<sup>&</sup>lt;sup>3</sup>Helmholtz Centre for Environmental Research, Leipzig, Germany

<sup>\*</sup>Corresponding author. ywang@sandia.gov

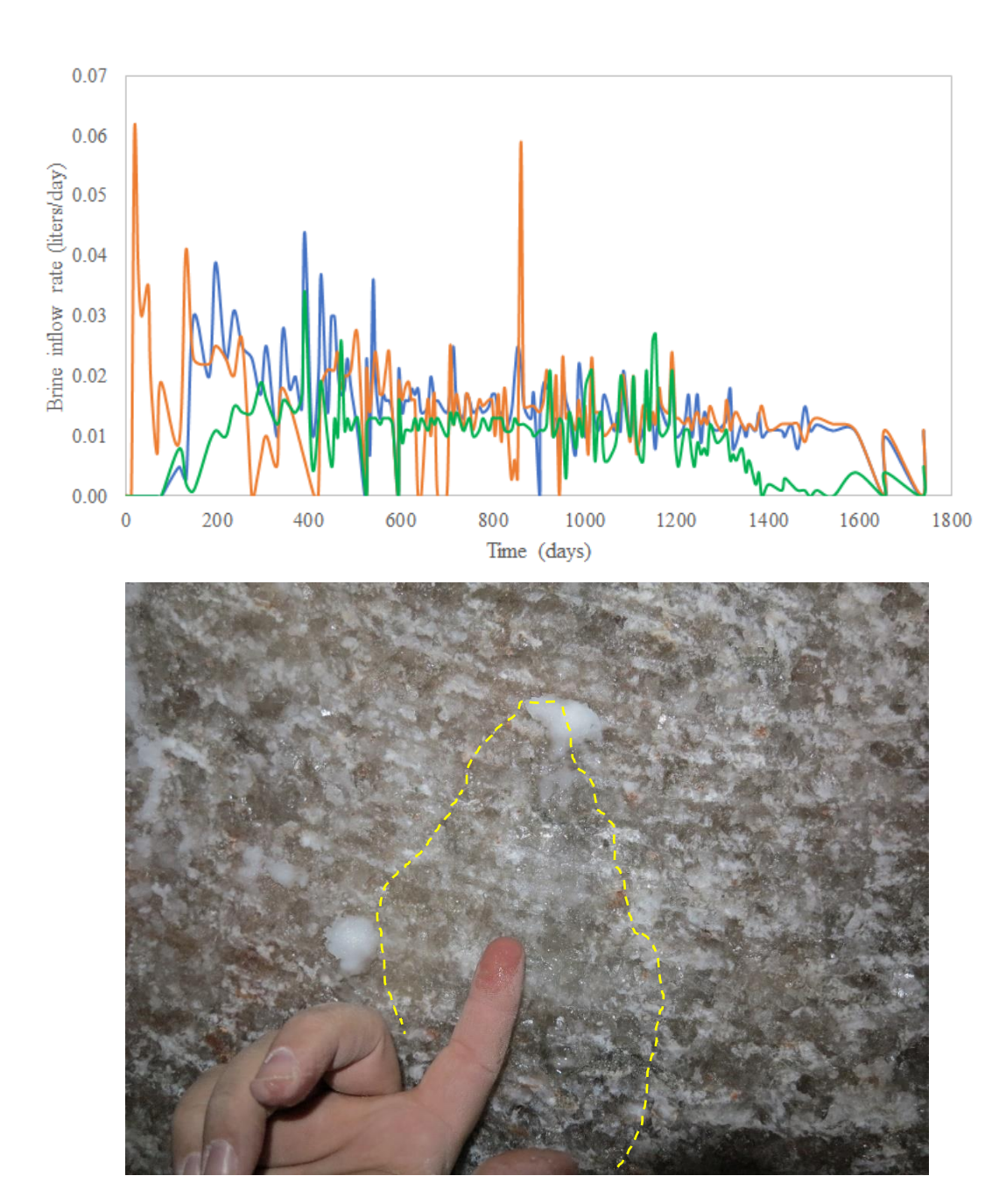


**Fig. 1.** (**A**) Brine inflow rates measured in different (as indicated by different colors) unheated boreholes<sup>37</sup> and (**B**) patch-wise brine wetting and weeping observed on tunnel surfaces (courtesy of Doug Weaver, Los Alamos National Lab) at the Waste Isolation Pilot Plant. In B, yellow dash line is added for visual guide.

below the static threshold. They attributed this anomaly to deformation-assisted fluid percolation. Watanabe<sup>6</sup> performed electrical impedance measurements on the deformation of fine-grained synthetic halide at 125 °C and 50 MPa confining pressure. The dihedral angle theory predicts an interconnected brine network not to form under these conditions. Nevertheless, the resistivity measurements indicated that the brine was interconnected at the pre-deformational stage. Further, the resistivity was found to increase with deformation, leading to a postulation that the brine might

exist as nanoscale thin films along grain boundaries. Popp and Kern<sup>7</sup> experimentally evaluated the effect of differential stress and mean confining stress on salt dilatancy and compaction. Given the dilatancy conditions constrained<sup>7</sup>, Schléder et al.<sup>8</sup> suggested that, at low differential and effective stresses, dilatancy could develop through microcracking as the pore fluid pressure increases near the lithostatic pressure. Creep closure in salt excavations could also generate an increase in fluid pressure, leading to diffuse dilatancy and an increase in salt permeability<sup>8</sup>. Shoenherr et al.<sup>9</sup> described the microstructure of halite for domal salt from the Infra-Cambrian Ara Group of the South Oman Salt Basin, close to an oil-bearing formation. Samples from the Ara salt formation indicate the presence of bitumen in microcracks and grain boundaries, suggesting the presence of a near-lithostatic fluid pressure for dilatancy and fluid permeation<sup>8,9</sup>. Shao et al.<sup>2</sup> summarized multiscale approaches for modeling fluid migration in salt. Using numerical simulations, they showed that pathway dilation along halite grain boundaries induced by a deviatoric stress created by an underground excavation might increase the permeability by two orders of magnitude.

Field measurements of fluid inflow into an underground opening reveal some key characteristics of fluid migration in salt. For instance, a field investigation program was carried out in a salt dome in northern Germany at a depth of 840 meters to quantify local hydrocarbon occurrences<sup>10</sup>. Twenty boreholes were drilled and the pressure and hydrocarbon inflow into the boreholes were monitored. Interestingly, the pressure buildup within the boreholes drastically, even for the boreholes less than one meter apart, thus strongly suggesting that the fluid might be compartmentalized into a relatively isolated patches in the formation. In addition, the fluid inflow in a borehole is generally episodic<sup>2</sup>. Similar behaviors were observed in the Waste Isolation Pilot Plant

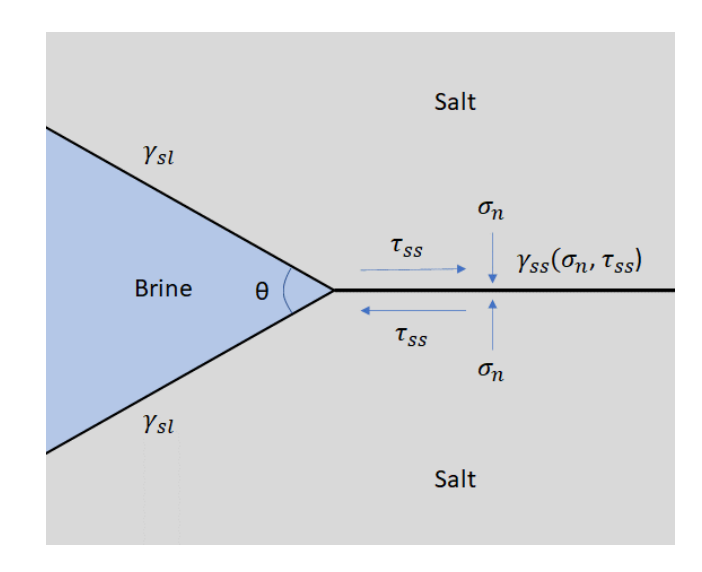


Fig. 2. Dihedral angle  $(\theta)$  as controlled by the stress along a grain boundary.

(WIPP), a deep geologic repository in a Permian bedded salt in the southern New Mexico, USA. Characteristic episodic brine releases into different sealed horizontal boreholes in the WIPP are shown in Figure 1A. Furthermore, direct observations on tunnel walls indicate that brine weeping in salt appears to occur in patches<sup>11</sup> (Figure 1B). In addition, brines obtained from repository drill holes are heterogenous in composition, indicating lack of mixing and fluid homogenization within the salt and during brine migration<sup>12</sup>. Thus, multiple lines of evidence suggest that fluids in salt formations are likely to be localized and fluid releases from such formations are generally episodic, though the underlying mechanism for these phenomena is unknown. It is interesting to notice that acoustic emissions are generally observed in brine migration and release<sup>13,14</sup>, indicating that fluid migration is closely associated with dynamic microstructural adjustments of salt. Therefore, The mechanism involved must be a coupled hydrological-mechanical process. Here we show that all the key characteristics observed in fluid distribution and migration are simply the manifestations of a porosity wave induced by a deviatoric stress in a deformable low-permeability medium.

### 2. Positive hydro-mechanical feedbacks

Let's consider how the stress state of a grain boundary affects the related dihedral angle. The dihedral angle  $\theta$  can be expressed by (Figure 2):

$$2\gamma_{sl}\cos\left(\frac{\theta}{2}\right) = \gamma_{ss} \approx \gamma_{ss}^{0}(\sigma_{n}) + k_{ss}\tau_{ss}^{2}$$
 (1)

where  $\gamma_{sl}$  is the surface tension of the liquid-solid interface;  $\gamma_{ss}$  is the surface tension of the solid-solid interface (i.e., the grain boundary);  $\tau_{ss}$  is the shear stress along the grain boundary;  $\sigma_n$  is the normal stress on the grain boundary;  $\gamma_{ss}^0$  is the surface tension of the grain boundary at  $\tau_{ss}=0$ ; and  $k_{ss}$  is a constant characterizing the elastic shear compliance of the grain boundary. In Equation (1), we assume that the surface tension of a grain boundary depends on the stress state of the boundary. In a compressive subsurface environment, for a given far-field stress,  $\sigma_n$  remains roughly constant since a thin water film along a grain boundary can sustain a normal stress 15, whereas  $\tau_{ss}$  could vary significantly due to the wetting and weakening of grain boundaries in the neighborhood as discussed below. The squared  $\tau_{ss}$  term on the right side of Equation (1) represents the contribution of strain energy to the surface tension (i.e., surface energy) of the solid-solid interface. Equation (1) indicates the dihedral angle decreases as the shear stress increases along

the grain boundary, thus enhancing grain boundary wetting and therefore the fluid network connectivity. Interestingly, in an olivine melting experiment, Bruhn et al. 16 demonstrated that shear deformation could interconnect a significant fraction of melt pockets, initially isolated under a hydrostatic condition, in polycrystalline olivine They matrix. postulated that, in dynamic a nonhydrostatic environment, intergranular melt percolation could be a viable mechanism for melt segregation and migration in the deep Earth.

Thus, the wetting state of a grain depends on both availability and shear stress along the boundary. It is reasonable to assume that boundary wetting grain significantly weaken the shear strength of boundary. This assumption consistent with the observation that the presence of a trace amount

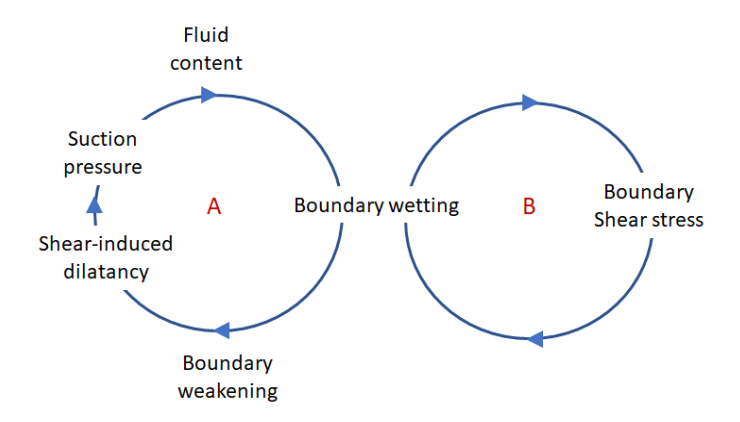


**Fig. 3.** Positive hydro-mechanical feedbacks postulated to exist in rock salt under a deviatoric stress. Feedback A involves grain boundary wetting, boundary weakening, shear-induced dilatancy, suction pressure and fluid content. Feedback B involves grain boundary wetting and boundary shear stress. Two coupled feedbacks gives rise to an overall positive feedback between the fluid content and the shear stress along dry grain boundaries.

intergranular water can significantly weaken rock salt<sup>17</sup>. For a given far-field stress, as a grain boundary becomes partially wetted, the shear stress tends to concentrate along the remaining dry segment of the boundary, thus causing more wetting along the boundary according to Equation

(1). Similarly, the wetting of one grain boundary would shift more shear stress to other boundaries in the neighborhood, resulting in more shear stress concentration and therefore more wetting in the neighborhood. At the same time, shear deformation opens more porosity of the material through so-called shear dilatancy<sup>18</sup>, which creates a suction pressure and thus forces more fluid into the weakened polycrystalline domain, thus further weakening the domain. Therefore, two positive hydro-mechanical feedbacks are postulated to operate in a salt formation under a deviatoric stress as shown in Figure 3. Feedback A controls the porosity evolution and fluid availability, while feedback B controls the fluid connectivity along grain boundaries. the two coupled feedbacks gives rise to an overall positive feedback between the fluid content and the shear stress along dry grain boundaries. As shown below, this overall feedback can lead to fluid localization and porosity wave formation. Popp and Kern<sup>7</sup> showed that a rock salt sample could undergo either dilatancy or compaction, depending on the relative magnitudes of the confining pressure and the deviatoric stress. In that sense, the proposed positive feedback is likely to occur in the dilatancy regime. Note that, though the dihedral angle-controlled wetting mechanism may be specific to a rock salt or partially molten rock system, the overall positive feedback postulated above between the fluid content and the shear stress along dry grain boundaries can apply to a more general set of deformable low-permeability geologic media including shale formations. In the rest of this paper, we will explore the dynamic implications of this overall feedback to fluid migration in such media.

#### 3. Model formulation

Let  $f_w$  denote the fraction of wet boundaries at a given spatial point. It is assumed that  $f_w$  is related to the fluid content (the porosity)  $\phi$  by:

$$f_w = \frac{\alpha \phi^m}{1 + \alpha \phi^m} \tag{2}$$

where  $\alpha$  and m (>0) are constants. This relationship ensures that  $f_w \to 0$  as  $\phi \to 0$  and  $f_w \to 1$  as  $\phi$  increases. Let the far-field stress to be specified by the two stress invariants:  $I' = \sigma_{ii}/3$  and  $J' = \sqrt{(\sigma_{11} - \sigma_{22})^2 + (\sigma_{22} - \sigma_{33})^2 + (\sigma_{33} - \sigma_{11})^2 + \sigma_{12}^2 + \sigma_{23}^2 + \sigma_{31}^2}$ , where  $\sigma_{ij}$  is a component of the far-field stress tensor. Equation (2) assumes the salt has no strength to hold open porosity that is not fluid filled. The partitioning of J' between dry and wet boundaries at a given spatial point can be described by:

$$J' = (1 - f_w^T)G_d \varepsilon_\tau' + f_w^T G_w \varepsilon_\tau'$$
(3)

where  $G_d$  and  $G_w$  are shear moduli of dry and wet grain boundaries, respectively, with  $G_w < G_d$ ;  $\varepsilon_\tau'$  is the shear strain at the given spatial point; and  $f_w^T$  is the weighted value of  $f_w$  over the neighborhood of the spatial point accounting for the influence of all wet grain boundaries in the neighborhood. For a one-dimensional system (Fig. 4):

$$f_w^T(X,t) = \int f_w(X',t)K(X-X')dX'$$

where *X* and *X'* are the spatial coordinates; and *K* is a kernel function with  $\int K(X - X')dX' = 1$ . The kernel function is isotropic and independent of location and vanishes as  $|X - X'| \to \infty$ . Based on this symmetry consideration,  $f_W^T$  can be expressed by (Wang and Budd, 2011)<sup>19</sup>:

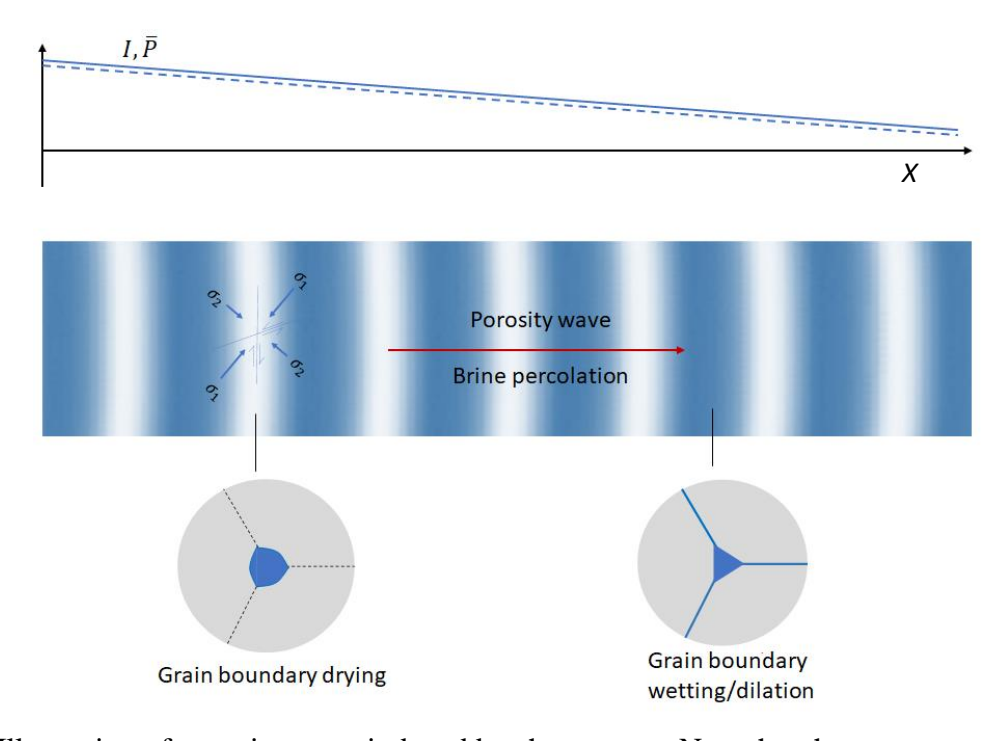


**Fig. 4.** Illustration of porosity wave induced by shear stress. Note that the stress can orient at any angle to the hydraulic gradient.

$$f_w^T \approx f_w + \beta' \frac{\partial^2 f_w}{\partial X^2} \tag{4}$$

where  $\beta'$  is a constant with  $\sqrt{\beta'}$  characterizing the influence distance of a weakened boundary on the other grain boundaries in the neighborhood.

Let  $\varepsilon_v$  denote the shear-induced dilatancy, which is a function of shear strain  $\varepsilon_\tau'$ . By expanding  $\varepsilon_v$  in powers of  $\varepsilon_\tau'$ , we have 18:

$$\varepsilon_{v}(\varepsilon_{\tau}') = \varepsilon_{v}(0) + D_{p}\varepsilon_{\tau}' + \frac{1}{2}R_{p}\varepsilon_{\tau}'^{2} + \cdots$$
 (5a)

where  $D_p$  and  $R_p$  are the coefficients of the expansion. By definition,  $\varepsilon_v(0) = 0$ ; and  $D_p = 0$  by the symmetry argument that the dilatancy remains the same whether  $\varepsilon_\tau'$  is positive or negative. Therefore, Equation (5a) can be reduced to:

$$\varepsilon_{\nu}(\varepsilon_{\tau}') \approx \frac{1}{2} R_{p} {\varepsilon_{\tau}'}^{2}$$
 (5b)

As shown in Equation (1), a grain boundary with a higher shear stress tends to draw the fluid from less stressed grain boundaries in the neighborhood, and this tendency is proportional to  $\tau_{ss}^2$  (equivalently to  $\varepsilon_{\tau}^{\prime 2}$ ). In this sense, Equation (5b) also captures the effect of shear stress on grain boundary wetting. Assuming a viscoelastic behavior for rock salt, we obtain the following momentum equation for the shear-induced porosity evolution:

$$\frac{\partial \phi}{\partial t} = \lambda' [\varepsilon_v E + (P' - I') - (\phi - \phi_0) E] \tag{6}$$

Where t is the time; E is the bulk Young's module of rock salt; P' is the hydraulic pressure;  $\phi_0$  is the porosity under no shear stress; and  $\lambda'$  is a constant characterizing the viscous behavior of salt. The first term in the square brackets represents the dilation force produced from shearing; the second term represents the effect of porewater pressure on salt volume expansion; and the third term represents the force to be overcome for the elastic expansion. The porosity evolution is also coupled to the fluid flow in salt:

$$\frac{\partial \phi}{\partial t} = \frac{\partial}{\partial X} \left( k \phi^3 \frac{\partial P'}{\partial X} \right) \tag{7}$$

where k is a constant characterizing the hydraulic conductivity of the salt. Darcy's flow is assumed for the fluid percolating in pores and along grain boundaries with a permeability proportional to  $\phi^3$  – a simplified Karman-Cozeny relationship for low porosity. This simplification will not change the linear stability analysis presented below. Equations (2-4, 5b, 6, 7) constitute a closed set of equations for a shear-induced fluid flow in the salt.

#### 4. Scaling

Let L denote the characteristic length of a system of interest and  $\overline{P}'$  the typical value of hydraulic pressure in the system. Adopting the following scaling factors:

$$T = \frac{L^2}{k\overline{P'}} \qquad \tau = \frac{t}{T} \qquad x = \frac{X}{L}$$

$$p = \frac{P}{\overline{P'}} \qquad \varepsilon_{\tau} = \frac{G_d \varepsilon_{\tau}'}{J'} \qquad I = \frac{I'}{\overline{P'}}$$

$$g = \frac{G_w}{G_d} \qquad \lambda = \frac{\lambda' T R_p E J'^2}{2G_d^2} \qquad \mu = \frac{2\overline{P} G_d^2}{R_d E J'^2}$$

$$\kappa = \frac{2G_d^2}{R_d J'^2} \qquad \beta = \frac{\beta'}{L^2} \qquad (8)$$

we can cast Equations (2-4, 5b, 6, 7) into:

$$\frac{\partial \phi}{\partial \tau} = \frac{\partial}{\partial x} \left( \phi^3 \frac{\partial p}{\partial x} \right) \tag{9}$$

$$\frac{\partial \phi}{\partial \tau} = \lambda [\varepsilon_{\tau}^2 + \mu(p - I) - \kappa(\phi - \phi_0)] \tag{10}$$

$$(1 + \alpha \phi^m) f_w = \alpha \phi^m \tag{11}$$

$$\varepsilon_{\tau} \left[ 1 - \left( f_w + \beta \frac{\partial^2 f_w}{\partial x^2} \right) (1 - g) \right] = 1 \tag{12}$$

It can be seen from the scaled equations that the system is determined by seven dimensionless parameter groups:  $\alpha$ ,  $\beta$ ,  $\lambda$ ,  $\mu$ ,  $\kappa$ , g and m. Except  $\beta$ , which will be constrained from field observations, all these parameters will be treated as adjustable parameters varying around one because of their scaled nature.

#### 5. Steady state

The steady state of Equations (9-12), indicated by overbars on the respective variables, can be solved from:

$$\frac{\partial}{\partial x} \left( \bar{\phi}^3 \frac{\partial \bar{p}}{\partial x} \right) = 0 \tag{13}$$

$$\bar{\varepsilon}_{\tau}^2 - \kappa(\bar{\phi} - \phi_0) = 0 \tag{14}$$

$$(1 + \alpha \bar{\phi}^m) \bar{f}_w = \alpha \bar{\phi}^m \tag{15}$$

$$\bar{\varepsilon}_{\tau} \left[ 1 - \bar{f}_{w} (1 - g) \right] = 1 \tag{16}$$

Given a generally low permeability of a salt formation, the pore fluid pressure in the formation is approximately equal to the lithostatic pressure, that is,  $\bar{p} \approx I$ . From Equation (13), we obtain:

$$\frac{\partial \bar{p}}{\partial x} = -q = \text{constant} \tag{17}$$

where q is the scaled porewater pressure gradient. All other variables remain uniform over the whole physical domain.

#### 6. Linear stability analysis

Linearizing Equations (9-12) around the steady state  $\bar{p}$ ,  $\bar{\phi}$ ,  $\bar{\varepsilon}_{\tau}$  and  $\bar{f}_{w}$  with respect to perturbations

$$p = \bar{p} + \delta p$$
$$\phi = \bar{\phi} + \delta \phi$$

$$\varepsilon_{\tau} = \bar{\varepsilon}_{\tau} + \delta \varepsilon_{\tau}$$

$$f_{w} = \bar{f}_{w} + \delta f_{w}$$
(18)

we obtain:

$$\frac{\partial \delta \phi}{\partial \tau} = \bar{\phi}^3 \frac{\partial^2 \delta p}{\partial x^2} - 3q\bar{\phi}^2 \frac{\partial \delta \phi}{\partial x} \tag{19}$$

$$\frac{\partial \delta \phi}{\partial \tau} = 2\lambda \bar{\varepsilon}_{\tau} \delta \varepsilon_{\tau} + \lambda \mu \delta p - \lambda \kappa \delta \phi \tag{20}$$

$$m\bar{f}_{w}(1-\bar{f}_{w})\delta\phi = \bar{\phi}\delta f_{w} \tag{21}$$

$$\delta \varepsilon_{\tau} = \bar{\varepsilon_{\tau}}^{2} (1 - g) \left( \delta f_{w} + \beta \frac{\partial^{2} \delta f_{w}}{\partial x^{2}} \right)$$
 (22)

Assume the perturbations to have the following form:

$$\delta p = \hat{p}e^{i\omega x + \zeta \tau} \qquad \qquad \delta \phi = \hat{\phi}e^{i\omega x + \zeta \tau}$$

$$\delta f_w = \hat{f}_w e^{i\omega x + \zeta \tau} \qquad \qquad \delta \varepsilon_\tau = \hat{\varepsilon}_\tau e^{i\omega x + \zeta \tau} \qquad (23)$$

where  $\omega$  is the wave number of the perturbation;  $\zeta$  is the growth rate of the perturbation; and i is the imaginary unit. Inserting the above expressions into Equations (19-22), we obtain the following homogenous algebraic equations:

$$\zeta \hat{\phi} = -\bar{\phi}^3 \omega^2 \hat{p} - 3q\bar{\phi}^2 \omega i \hat{\phi} \tag{24}$$

$$\zeta \hat{\phi} = 2\lambda \bar{\varepsilon}_{\tau} \hat{\varepsilon}_{\tau} + \lambda \mu \hat{p} - \lambda \kappa \hat{\phi} \tag{25}$$

$$m\bar{f}_w(1-\bar{f}_w)\hat{\phi} = \bar{\phi}\hat{f}_w \tag{26}$$

$$\hat{\varepsilon}_{\tau} = \bar{\varepsilon}_{\tau}^{2} (1 - g)(1 - \beta \omega^{2}) \hat{f}_{w} \tag{27}$$

For a nontrivial solution of the equations (i.e., for a nonzero perturbation to be permitted) the determinant of the coefficient matrix of the equations must be zero:

$$\begin{vmatrix}
\zeta + 3q\bar{\phi}^{2}\omega i & \bar{\phi}^{3}\omega^{2} & 0 & 0 \\
\zeta + \lambda\kappa & -\lambda\mu & 0 & -2\lambda\bar{\varepsilon}_{\tau} \\
m\bar{f}_{w}(1 - \bar{f}_{w}) & 0 & -\bar{\phi} & 0 \\
0 & 0 & -\bar{\varepsilon}_{\tau}^{2}(1 - g)(1 - \beta\omega^{2}) & 1
\end{vmatrix} = 0 \quad (28)$$

Solving Equation (28) for  $\zeta$ , we finally obtain the dispersion equation that relates the growth of a perturbation to its wave number:

$$\zeta(\omega) = \frac{2m\lambda\bar{\phi}\bar{\varepsilon}_{\tau}^{3}\bar{f}_{w}(1-\bar{f}_{w})(1-g)(1-\beta\omega^{2})\omega^{2} - \lambda\kappa\bar{\phi}^{3}\omega^{2} - 3\lambda\mu q\bar{\phi}^{2}\omega i}{\lambda\mu + \bar{\phi}^{3}\omega^{2}}$$
(29)

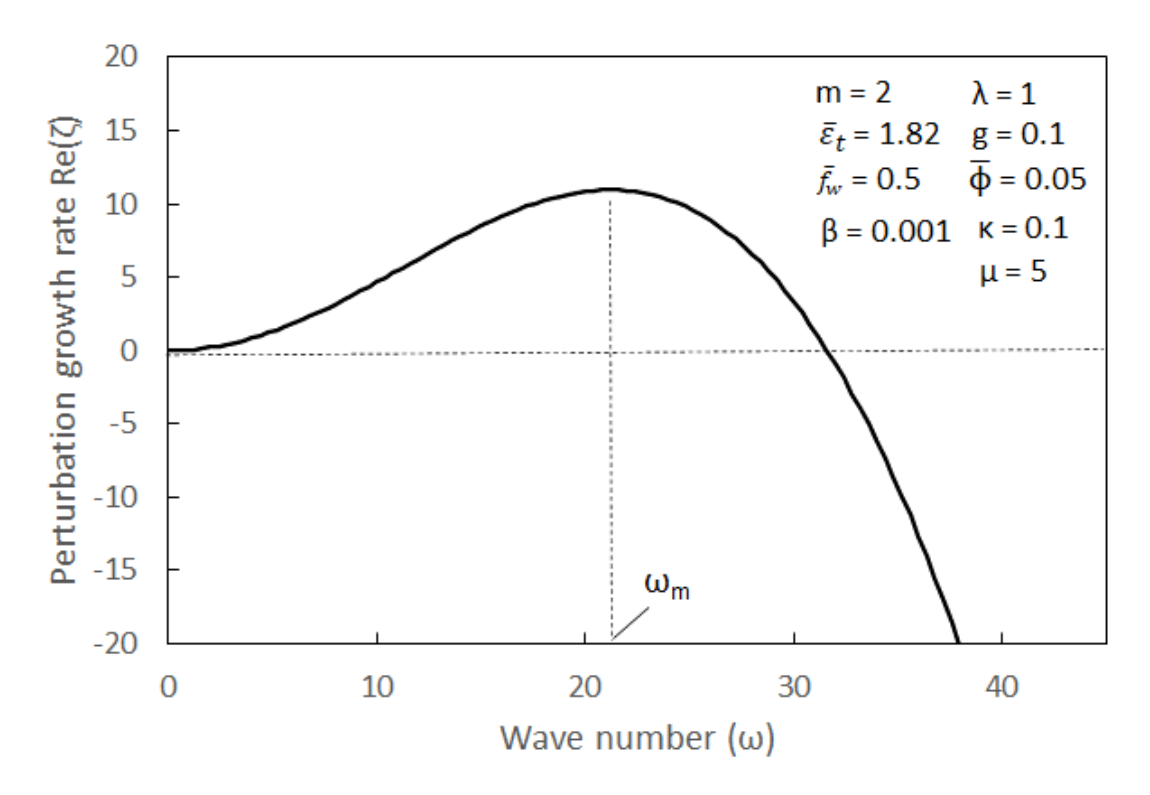


**Fig. 5.** Growth rate of perturbation as a function of wave number. Existence of a positive growth rate implies the instability of the system and thus the formation of a porosity wave.

The real part of  $\zeta(\omega)$ ,  $\text{Re}(\zeta)$ , represents the actual growth rate of a perturbation, while the imaginary part,  $\text{Im}(\zeta)$ , indicates a temporal oscillation of a spatial pattern<sup>19</sup>. A positive  $\text{Re}(\zeta)$  means that the perturbation with the corresponding wave number tends to grow with time, leading to the emergence of a spatial repetitive pattern. As shown in Figure 5, under appropriate stress and hydraulic conditions, there exist positive  $\text{Re}(\zeta)$  values for certain wave numbers, implying self-organized pattern formation. That is, an infinitesimal perturbation to an initially uniform fluid distribution in a salt formation can be amplified through the proposed hydro-mechanical feedback, and consequently the fluid can autonomously partition into spatially isolated patches. If a hydraulic gradient exists  $(q \neq 0)$ , the term  $\text{Im}(\zeta)$  is nonzero. From Equation (23), this means that the

porosity and other variables in the system oscillate with time at a given spatial point, implying that these fluid patches move down the pressure gradient as a porosity wave<sup>20</sup>, leading to the episodic fluid release observed in an underground opening (Figure 1A)<sup>2</sup>. In the absence of any hydraulic gradient, the term  $\text{Im}(\zeta)$  becomes zero, and the porosity wave becomes stationary. Consequently, the fluid would be spatially localized in relatively isolated patches as inferred from field observations<sup>10</sup> (Figure 1B). Here each patch of fluid is defined as an interconnected network of fluid-filled grain boundaries and pores.

From the imaginary part of  $\zeta(\omega)$  in Equation (29), the phase velocity  $(v_{\text{wave}})$ , of a porosity wave with wave number  $\omega$  is estimated to be:

$$v_{\text{wave}} = \frac{3\lambda\mu q\bar{\phi}^2\omega}{2\pi(\lambda\mu + \bar{\phi}^3\omega^2)} \cdot \frac{2\pi}{\omega} \frac{L}{T} = \frac{3\lambda\mu q\bar{\phi}^2}{\lambda\mu + \bar{\phi}^3\omega^2} \cdot \frac{L}{T}$$
(30)

where term  $\frac{3\lambda\mu q\bar{\phi}^2\omega}{2\pi(\lambda\mu+\bar{\phi}^3\omega^2)}$  represents the number of wave cycles passing through a given spatial point within a unit scaled time; term  $\frac{2\pi}{\omega}$  represents the scaled wave length; and factor  $\frac{L}{T}$  is used to scale the scaled flow velocity back to the actual spatial and temporal coordinates. For  $\lambda\mu\gg\bar{\phi}^3\omega^2$ , i.e., for a purely elastic medium  $(\lambda\to\infty)$ ,  $v_{\rm wave}$  is reduced:

$$v_{\text{wave}} = 3q\bar{\phi}^2 \cdot \frac{L}{T} \tag{31}$$

 $v_{\rm wave}$  becomes independent of  $\omega$ , implying that no dispersion occurs, i.e., the waves with different numbers propagate at the same speed. However, for  $\lambda\mu\sim\bar\phi^3\omega^2$ , the phase velocity of a porosity wave rapidly decreases with the wave number ( $\propto\omega^{-2}$ ) and consequently a long wave moves faster than a short wave. The viscosity of a viscoelastic medium (low  $\lambda$ ) tends to filter out high frequency waves.

#### 7. Wavelength, time interval of fluid release and enhanced fluid flux

A purely elastic case is now considered by making  $\lambda \to \infty$ . Equation (29) is reduced to:

$$\zeta(\omega) = \frac{2m\bar{\phi}\bar{\varepsilon}_{\tau}^{3}\bar{f}_{w}(1-\bar{f}_{w})(1-g)(1-\beta\omega^{2})\omega^{2} - \kappa\bar{\phi}^{3}\omega^{2} - 3\mu q\bar{\phi}^{2}\omega i}{\mu}$$
(32)

The wave number corresponding to the maximum  $\text{Re}(\zeta)$ ,  $\omega_m$ , dictates the actual wavelength of porosity wave. From Equation (32), by setting  $\frac{d\zeta}{d\omega} = 0$ , we obtain:

$$\omega_{m} = \sqrt{\frac{2m\bar{\varepsilon}_{\tau}^{3}\bar{f}_{w}(1-\bar{f}_{w})(1-g) - \kappa\bar{\phi}^{2}}{4m\beta\bar{\varepsilon}_{\tau}^{3}\bar{f}_{w}(1-\bar{f}_{w})(1-g)}}$$
(33)

The result indicates the condition for the system to be unstable (i.e., for a porosity wave to emerge) is:

$$2m\bar{\varepsilon}_{\tau}^{3}\bar{f}_{w}(1-\bar{f}_{w})(1-g) > \kappa\bar{\phi}^{2}$$
 (34)

Clearly, the conditions that favor the formation of a porosity wave include large shear strain  $(\bar{\varepsilon}_{\tau})$ , half-wet grain boundary  $(\bar{f}_w)$ , high contrast in shear strength between wet and dry grain boundaries (g), low moduli  $(\kappa)$ , and low porosity  $(\bar{\phi})$ . Under a large shear strain, Equation (33) becomes:

$$\omega_m \approx \sqrt{\frac{1}{2\beta}}$$
 (35)

The wavelength of the porosity wave is estimated to be:

$$L_{\text{wave}} = \frac{2\pi}{\omega_m} L \approx 2\pi \sqrt{2\beta'}$$
 (36)

As mentioned earlier (Equation 4),  $\sqrt{\beta'}$  characterizes the influence distance of a weakened point on the stress state of its neighborhood. Equation (34) quantifies the wavelength of a porosity wave as ~ 9 times that distance. The influence distance can roughly be constrained from the extent of disturbed rock zone around a subsurface opening, which is estimated to range from centimeters around a borehole<sup>21</sup> to meters around an underground tunnel<sup>22</sup>. Considering the size of a fluid patch is half its wavelength (i.e., a full wavelength contains one dry domain and one wet domain), the size of individual fluid patches in a salt formation is estimated to range from decimeters to tens of meters.

The time interval for episodic fluid release  $(t_p)$  can be estimated from Equations (31) and (36):

$$t_p = \frac{L_{\text{wave}}}{v_{\text{wave}}} = \frac{2\pi L^2}{3q\bar{\phi}^2 \omega_m k \bar{P}'}$$
 (37)

In the above equation, parameter q is a scaled pressure gradient and approximately unity. To account for the effect of shear-induced dilatancy,  $\bar{\phi}$  is set to be ~ 0.1. The hydraulic conductivity [i.e.,  $k\phi^3$  in Eq. (7)] of rock salt with a porosity of 1-2% ranges from  $10^{-15}$  to  $10^{-14}$  m/s<sup>21</sup>, which corresponds to the k value of  $5 \times 10^{-9}$  to  $10^{-8}$  m/s. Let's consider fluid release from a salt horizon at a depth of 500 meters, corresponding to the  $\bar{P}'$  value of ~ 1000 m. Let's choose  $\omega_m$  to be ~ 10. In addition, as discussed above, a typical length of a porosity wave ranges from 0.1 to 10 meters. Plugging all the parameter values into Equation (37), we estimate the interval of fluid release to range from hours to years, consistent with field observations (Figure 1).

The fluid flux is constituted of two components: (1) the fluid moving as porosity wave pockets and (2) the fluid percolating as a Darcy's flow between the pockets. The first component can be approximately expressed as  $\bar{\phi}v_{\rm wave} \approx 3q\bar{\phi}^3L/T$ . From Equations (13) and (17), the

second component can be expressed as  $q\bar{\phi}^3L/T$ . Therefore, the total fluid flux,  $F_{wave}$ , is estimated to be  $4q\bar{\phi}^3L/T$ . From Equation (14), we have:

$$F_{wave} \approx 4q \left(\phi_0 + \frac{\bar{\varepsilon}_{\tau}^2}{\kappa}\right)^3 \frac{L}{T}$$
 (38)

Note that the Darcy's flow under no shear-induced porosity wave is  $q\phi_0^3L/T$ . The enhancement factor of fluid flux by porosity wave  $(f_e)$  is estimated to be:

$$f_e = 4\left(1 + \frac{\bar{\varepsilon}_\tau^2}{\phi_0 \kappa}\right)^3 \tag{39}$$

That is, the emergence of shear-induced porosity wave can enhance the fluid flux by a factor of at least 4, and this enhancement increases rapidly with the shear strain. This result is consistent with the work by Shao et al.<sup>2</sup>, which shows that pathway dilation along halite grain boundaries induced by a deviatoric stress created by an underground excavation might increase the permeability by two orders of magnitude.

One would guess that this enhancement could mainly be caused only by a uniform dilation of the medium by shear strain. But this seems unlikely. As shown in Equation (34), as the shear strain increases, the criterion for the occurrence of a porosity wave becomes met quickly. That is, the dilation and the emergence of a porosity wave likely go hand in hand. In addition, a subsurface environment is generally volume-constrained and tends to limit the development of a uniform dilation. A fluid flow in a porous medium can be viewed as an energy dissipation process. Thus, the emergence of a porosity wave may be the most efficient way for the system to move a fluid through a low-permeability deformable media with minimum total volume expanded.

#### 8. Discussion

The above analysis indicates possible emergence of a porosity wave under a deviatoric stress in a salt formation. Such a wave can significantly enhance a fluid flow in low-permeability salt. A salt dome is generally subjected to a relatively large shear stress during its formation<sup>23</sup>. Through porosity waves, on one hand, the fluid in a salt dome can relatively easily be squeezed out, rendering domal salt relatively dry as compared to bedded salt, as observed<sup>23</sup>. On the other hand, fluids underneath a salt dome may be able to infiltrate into the salt via a porosity wave, and the infiltrated fluids may then be compartmentalized into isolated patches as indicated by field observations<sup>10</sup>. As shown above, a porosity wave stems from shear localization. Internal flow banding is commonly observed in Gulf Coast salt domes<sup>24</sup>. The banding is generally dragged parallel with boundary shear zones or the edge of salt during salt dome ascending. Such banding clearly indicates the common occurrence of shear localization in salt dome intrusion and can be viewed as indirect evidence for the possible existence of a porosity wave in a salt formation.

Two key physical and chemical characteristics have been observed to associate with porosity wave propagation. First, it is known that shear and shear-induced dilatancy of granular materials would cause acoustic emissions<sup>25</sup>. As a porosity wave propagates, the salt structure

would experience dynamic shearing, dilation, and contraction, resulting in acoustic emissions, as observed <sup>13,14</sup>. Second, unlike a conventional Darcy's flow, as a porosity wave propagates, the fluid in each patch remains relatively isolated with minimal mixing between neighboring patches. Abitz et al. <sup>12</sup> show that brines obtained from WIPP repository drill holes are heterogenous in composition, indicating a lack of mixing and fluid homogenization within the salt and during migration. Thus, the concept of porosity wave provides a consistent explanation for the key features observed in fluid distribution and release in salt formations.

The concept of porosity wave may have implications to other geologic systems. Stress-driven, especially shear-induced, melt extraction from a highly deformed, partially molten rock has been considered as a plausible mechanism to produce the observed disequilibrium between the crust-forming lavas and their mantle sources<sup>26</sup>. It was found that an instability can occur in the compaction of a porous medium via a positive feedback in which a reduction in viscosity of the medium with increasing porosity in a region would result in a decrease in the melt pressure, which in turn attracts more melt to the region<sup>27-31</sup>. Different from that mechanism, the concept of porosity wave proposed here is based on shear-induced grain boundary wetting/drying and material dilatancy. Fluid extraction by a porosity wave can take place at a very early stage, even when the medium remains elastic as long as a high enough shear stress is imposed.

A compaction-driven porosity wave - a single or multiple over-pressurized pockets of high porosity self-propagating vertically by buoyancy during sediment compaction and diagenesis <sup>32,33</sup> - has been considered as a mechanism for fluid expulsion and migration in sedimentary basins. Unlike such waves, the porosity wave postulated here is a sustainable train of repetitive porosity patterns autonomously arising from positive feedbacks among intergranular wetting, grain boundary weakening and shear-induced material dilation. These positive feedbacks are general enough that they can be applied to other low-permeability deformable media such as shale. Shale is generally considered as an impermeable caprock for a conventional oil/gas reservoir or a subsurface gas (CO<sub>2</sub>, H<sub>2</sub> or CH<sub>4</sub>) storage system <sup>34,35</sup>. However, if the proposed mechanism is confirmed, the assumed functionality of shale as a caprock formation needs to be reexamined. The suggested mechanism may also help address the paradox in oil/gas generation that a large volume of hydrocarbon fluids has been expelled from low-permeability shale source rocks <sup>36</sup>. Furthermore, the suggested concept provides an insight into designing a new strategy for fluid extraction from or injection into a shale formation.

Similarly, the suggested mechanism may need to be considered in a performance assessment of a nuclear waste geologic repository in a salt or shale formation, especially for domal salt, which is generally subjected to a high shear deformation. As discussed earlier, a porosity wave arises from shear-induced grain boundary wetting, weakening and dilatancy. The propagation of such a wave is driven by a hydraulic gradient. During an operational period of a repository, certain volumes of fluid inflow may occur due to a hydraulic gradient created by an underground excavation. However, after the repository closure, the stress state and hydraulic condition of a repository will gradually return to the original, nearly isotropic stress state. Consequently, the fluid flow in the repository system is expected to abate, transitioning from a propagating porosity wave to a stationary wave.

#### 9. Conclusions and perspective

Using a linear stability analysis, we have shown that a porosity wave can autonomously emerge from positive feedbacks among intergranular wetting, grain boundary weakening and shear-induced material dilation. Generally observed fluid localization or episodic fluid release can be viewed respectively as a stationary or a propagating shear-induced porosity wave. The analysis shows that the velocity of fluid flow can be significantly enhanced by the emergence of a porosity wave. Our model provides a consistent prediction of the occurrence of episodic brine release and the spatial and temporal scales for brine compartmentalization and release in rock salt. Such a porosity wave is expected to occur in a general category of low-permeability deformable media (e.g., salt, shale, partially molten rocks, etc.) in the presence of a deviatoric stress. The result may provide an insight into designing a new engineering approach to fluid injection into or extraction from unconventional reservoirs.

The concept and the related model developed here provide a theoretical framework for modeling fluid flows in deformable low-permeability media. However, we want to point out that the model at the current stage has its own limitations and the linear stability analysis performed can only capture the nonlinear dynamics near a steady state. To understand the full nonlinear dynamics of the system, a numerical solution of the equations is required, which will be a future research activity. The existing model can be improved at least in following aspects:

- Expand the model to explicitly include the evaluation of local stress fields. To do so, the model needs to be extended to a 2-D or 3-D system.
- Systematically and numerically solve the expanded model for more realistic physical domains and boundary conditions to simulate the emergence of porosity waves under various shear conditions.
- Design and perform controlled experiments to better constrain the related model parameters.
- Use the improved model to simulate field scale experiments and test the results against field observations.

#### 10. Nomenclatures

$D_p$	Coefficient of the expansion of $\varepsilon_v$
$\dot{E}$	Bulk Young's module of rock salt
$F_{wave}$	Total fluid flux in the presence of a porosity wave
$f_e$	Enhancement factor of fluid flux by a porosity wave
$f_{w}$	Fraction of wet boundaries at a given spatial point
$f_w \\ f_w^T$	Weighted value of $f_w$ over the neighborhood of a spatial point
$G_d$	Shear moduli of dry grain boundaries
$G_w$	Shear moduli of wet grain boundaries
g	Ratio of $G_w$ to $G_d$
I	Scaled I'
I'	Stress invariant $(\sigma_{ii}/3)$
J'	Stress invariant $(\sqrt{(\sigma_{11} - \sigma_{22})^2 + (\sigma_{22} - \sigma_{33})^2 + (\sigma_{33} - \sigma_{11})^2 + \sigma_{12}^2 + \sigma_{23}^2 + \sigma_{31}^2})$
K	Kernel function
k	Constant characterizing the hydraulic conductivity of salt

$k_{ss}$	Constant characterizing the elastic shear compliance of the grain boundary
L	Characteristic length
$L_{ m wave}$	Wavelength of a porosity wave
m	Constant in Eq. (2)
$_{-}^{P^{\prime}}$	Hydraulic pressure
$\overline{P}'$	Typical value of hydraulic pressure
p	Scaled P'
q	Scaled porewater pressure gradient
$R_p$	Coefficient of the expansion of $\varepsilon_v$
T	Characteristic time scale
t	Time
$t_p$	Time interval for episodic fluid release
$v_{ m wave}$	Phase velocity of a porosity wave
X	Spatial coordinate
X	Scaled X
α	Constant in Eq. (2)
$\beta$	Scaled $eta'$
eta'	Constant characterizing the influence distance of a weakened boundary on the other
0	grain boundaries in the neighborhood
$\gamma_{ss}^0$	Surface tension of the grain boundary at $\tau_{ss} = 0$
$\varepsilon_v$	Shear-induced dilatancy
$arepsilon_{ au}^{\prime}$	Scaled $\varepsilon_{\tau}'$ shear strain
$\zeta$	Growth rate of a perturbation
τ	Scaled t
$ au_{SS}$	Shear stress along the grain boundary
K	Dimensionless parameter group $2G_d^2/R_dJ'^2$
λ	Dimensionless parameter group $\lambda' T R_p E J'^2 / 2G_d^2$
$\lambda'$	Constant characterizing the viscous behavior of salt
μ	Dimensionless parameter group $2\bar{P}G_d^2/R_dEJ'^2$
•	Component of the far-field stress tensor
$\sigma_{ij}$	Normal stress on the grain boundary
$\sigma_n \ \omega$	Wave number of a perturbation
$\omega_m$	Preferred wave number
$\phi$	Porosity
$\overset{arphi}{\phi}_0$	Porosity under no shear stress
$\theta$	Dihedral angle
-	· · · · · · · · <del>0</del>

**Acknowledgments:** Sandia National Laboratories is a multi-mission laboratory managed and operated by National Technology and Engineering Solutions of Sandia, LLC., a wholly owned subsidiary of Honeywell International, Inc., for the U.S. Department of Energy's National Nuclear Security Administration under contract DE-NA-0003525. The work was supported by DOE Spent Fuel Waste Science & Technology (SFWST) Program. This work is also supported by DOE Fossil Energy Fundamental Shale Research Program. The authors thank the DECOVALEX Funding

Organizations Andra, BGR, CNSC, US DOE, ENSI, JAEA, IRSN, KAERI, NWMO, RWM, SURAO, SSM and Taipower for their technical support. We would like to thank anonymous reviewer 1 for his detailed review and constructive comments, which have greatly help improve the manuscript.

#### 11. References

- 1. Hansen, F. D.; Leigh, C. D., 2011, *Salt Disposal of Heat-Generating Nuclear Waste*, Sandia National Laboratories, Albuquerque, New Mexico, USA. SAND2011-0161.
- 2. Shao, H., Wang, Y., Kolditz, O., Nagel, T., Brüning, T., 2019, Approaches to multi-scale analyses of mechanically and thermally-driven migration of fluid inclusions in salt rocks, *Phys. Chem. Earth*, 113, 1-13.
- 3. Ghanbarzadeh, S., Prodanović, M., Hesse, M. A., 2014, Percolation and grain boundary wetting in anisotropic texturally equilibrated pore networks, *Physical Review Letters*, 113, 048001.
- 4. Lewis, S., Holness, M., 1996, Equilibrium halite-H<sub>2</sub>O dihedral angles: High rock-salt permeability in the shallow crust? *Geology*, 24 (5), 431–434.
- 5. Ghanbarzadeh, S., Hesse, M. A., Prodanović, M., Gardner, J. E., 2015, Deformation-assisted fluid percolation in rock salt, *Science*, 350, 1069-1072.
- 6. Watanabe, T., 2010, Geometry of intercrystalline brine in plastically deforming halite rocks: inference from electrical resistivity, in: M. I. Spalla, A. M. Marotta, G. Gosso (eds.) Advances in Interpretation of Geological Processes: Refinement of Multi-scale Data and Integration in Numerical Modeling. Geological Society, London, Special Publications. 332, 69-78.
- 7. Popp, T., Kern, H., 2001, Evolution of dilatancy and permeability in rock salt during hydrostatic compaction and triaxial deformation, *J. Geophysical Research*, 106, 4061-4078,
- 8. Schléder, Z., Urai, J. L., Nollet, S., Hilgers, C., 2008, Solution-precipitation creep and fluid flow in halite: a case study of Zechstein (Z1) rocksalt from Neuhof salt mine (Germany). *Int. J. Earth Sci (Geol Rundsch)*, 97, 1045–1056.
- 9. Schoenherr, J., Urai, J. L., Kukla, P. A., Littke, R., Schleder, Z., Larroque, J.-M., Newall, M. J., Al-Abry, N., Al-Siyabi, H. A., Rawahi, Z., 2007, Limits to the sealing capacity of rock salt: A case study of the infra-Cambrian Ara Salt from the South Oman salt basin. *AAPG Bulletin*, 91, 1541-1557.
- 10. Paul, B., Shao, H. Hesser, J., Lege, C., 2015, In situ quantification of hydrocarbon in an underground facility in tight salt rock, in: G. Lollino, D. Giordan, K. Thuro, C. Carranza-Torres, F. Wu, P. Marinos, C. Delgado, Eds., *Engineering Geology for Society and Territory Volume 6 Applied Geology for Major Engineering Projects*, Spinger, p. 893-896.
- 11. Deal, D.E., Abitz, R. J., Myers, J., Belski, D. S., Martin, M. L., Milligan, D. J., Sobocinski, R.W., James Lipponer. P. P., 1993, *Brine Sampling and Evaluation Program 1991 Report*. Carlsbad, NM, US Department of Energy WIPP Project Office, DOE-WIPP 93–026.
- 12. Abitz, R. Myers, J., Drez, P., Deal, D., 1990, Geochemistry of Salado formation brines recovered from the waste isolation pilot plant (WIPP) repository, *Waste management 90: working towards a cleaner environment: waste processing, transportation, storage and*

- disposal, technical programs and public education, Tucson, Arizona, USA, 25 Feb 1 Mar 1990.
- 13. Kuhlman, K., Mills, M., Jayne, R., Matteo, E., Herrick, C., Nemer, M., Xiong, Y., Choens, C., Paul, M., Stauffer, P., Boukhalfa, H., Guiltinan, E., Rahn, T., Weaver, D., Otto, S., Davis, J., Rutqvist, J., Wu, Y., Hu, M., Uhlemann, S., Wang, J., 2021, *Brine Availability Test in Salt (BATS) FY21 Update*, Sandia National Laboratories, Albuquerque, New Mexico, USA. SAND2021-10962 R.
- 14. Rothfuchs, T., Wieczorek, K., Feddersen, H.K., Staupendahl, G., Coyle, A.J., Kalia, H., Eckert, J., 1988, *Brine Migration Test: Asse Salt Mine Federal Republic of Germany Final Report*, GSF- Bericht 6/88, Joint project between Office of Nuclear Waste Isolation (ONWI) and Gesellschaft für Strahlen- und Umweltforschung Munchen (GSF).
- 15. Renard, F., Ortoleva, P., 1997, Water films at grain-grain contacts: Debye-Hückel, osmotic model of stress, salinity, and mineralogy dependence, *Geochim. Cosmochim. Acta*, 61, 1963–1970.
- 16. Bruhn, D., Groebner, N., Kohlstedt, 2000, An interconnected network of core-forming melts produced by shear deformation, *Nature*, 403, 883-886.
- 17. Urai, J. L., Spiers, C. J., Zwart, H. J., Lister, G. S., 1986, Weakening of rock salt by water during long-term creep, *Nature*, 324, 554-557.
- 18. Tighe, B. P., 2014, Shear dilatancy in marginal solids, *Granular Matter*, 16, 203-208.
- 19. Wang, Y., Budd, D. A., 2011, Stress-induced chemical waves in sediment burial diagenesis, *Nature Communications*, 3, 685/DOI:10.1038/ncomms1684.
- Wang, Y., Chan, M. A., Merino, E., 2015, Self-organized iron-oxide cementation geometry as an indicator of paleo-flows, *Scientific Reports*, 5:10792 | DOi: 10.1038/srep10792.
- 21. Shao, H., Wang, Y., Nagel, T., Kolditz, O., Yoshioka, K., 2020, Determination of permeability for hydrocarbon release due to excavation-induced stress redistribution in rock salt, *International Journal of Rock Mechanics & Mining Sciences*, 136, 104525.
- 22. Hansen, F. D., 2003, *The Disturbed Rock Zone at the Waste Isolation Pilot Plant*, Sandia National Laboratories, Albuquerque, New Mexico, USA. SAND2003-3407.
- 23. Hansen, F. D., Kuhlman, K. L., Sobolik, S., 2016, Considerations of the Differences between Bedded and Domal Salt Pertaining to Disposal of Heat-Generating Nuclear Waste, Sandia National Laboratories, Albuquerque, New Mexico, USA. SAND2016-6522R.
- 24. Looff, K. M., Looff, K. M., Rautman, C., 2010, Inferring the geologic significance and potential impact of salt fabric and anomalous salt on the development and long-term operation of salt storage caverns on Gulf coast salt domes, Solution Mining Research Institute Spring 2010 Technical Conference Grand Junction, Colorado, USA, 26-27 April 2010.
- 25. Siman-Tov, S., Brodsky, E. L., 2021, Distinguishing between rheophysical regimes of fluid-saturated granular-flows using dilatancy and acoustic emission measurements, *Granular Matter.*, 23, 44.
- 26. Kohlstedt, D. L., Holtzman, B. K., 2009, Hearing melt out of the Earth: An experimentalist's perspective on the influence of deformation on melt extraction, Annu. Rev. Earth Planet. Sci., 37, 561-593.
- 27. McKenzie, D., 1984, The generation and compaction of partially molten rock, J. Petrology, 25, 713-765.
- 28. Stevenson, D. J., 1989, Spontaneous small-scale melt segregation in partial melts undergoing deformation. *Geophysical Research Letter*, 16, 1067-1070.

- 29. Spiegelman, M., 1993, Physics of melt extraction: theory, implications and applications, *Phil. Trans. R. Soc. Lond. A.*, 342, 23-41.
- 30. Katz, R. F., Spiegelman, M., Holtzman, B., 2006, The dynamics of melt and shear localization in partially molten aggregates, Nature, 442, 676-679.
- 31. Weinberg, R. F., Veveakis, E., Regenauer-Lieb, K., 2015, Compaction-driven melt segregation in migmatities, *Geology*, 43 (6), 471–474.
- 32. Connolly, J. A. D., Podladchikov, Y. Y., 1998, Compaction-driven fluid flow in viscoelastic rock. *Geodin. Acta*, 11, 55-84.
- 33. L'Heureux, I., 2018, Diagenetic Self-Organization and Stochastic Resonance in a Model of Limestone-Marl Sequences, *Geofluids*, 2018, 4968315, 18 pages.
- 34. Al-Bazali, T. M., Zhang, J., Chenevert, M. E., Sharma, M. M., 2005, Measurement of the Sealing Capacity of Shale Caprocks, *SPE Annual Technical Conference and Exhibition*, Dallas, Texas, October 2005. Paper Number: SPE-96100-MS
- 35. Olabode, *A.*, Bentley, *L.*, Radonjic, M., 2012, Shale caprock integrity under carbon sequestration conditions, *AIP Conference Proceedings*, 1453, 347-352.
- 36. Mackenzie, A. S., Leythaeuser, D., Schaefer, R. G., 1983, Expulsion of petroleum hydrocarbons from shale source rocks, *Nature*, 31, 506-509.
- 37. Kuhlman, K. L., Mills, M. M., Matteo, E. N., 2017, *Consensus on Intermediate Scale Salt Field Test Design*, Sandia National Laboratories, Albuquerque, New Mexico, USA. SAND2017-3179R.